




Influence of field amplitude and dipolar interactions on the dynamic response of immobilized magnetic nanoparticles: Perpendicular mutual alignment of an alternating magnetic field and the easy axes

Alexander V. Ambarov , Vladimir S. Zverev , and Ekaterina A. Elfimova *

*Department of Theoretical and Mathematical Physics, Institute of Natural Sciences and Mathematics,
Ural Federal University, 51 Lenin Avenue, Ekaterinburg 620000, Russia*



(Received 9 November 2022; accepted 11 January 2023; published 2 February 2023)

In this paper, the dynamic magnetic properties of an ensemble of interacting immobilized magnetic nanoparticles with aligned easy axes in an applied ac magnetic field directed perpendicular to the easy axes are considered. The system models soft, magnetically sensitive composites synthesized from liquid dispersions of the magnetic nanoparticles in a strong static magnetic field, followed by the carrier liquid's polymerization. After polymerization, the nanoparticles lose translational degrees of freedom; they react to an ac magnetic field via Néel rotation, when the particle's magnetic moment deviates from the easy axis inside the particle body. Based on a numerical solution of the Fokker-Planck equation for the probability density of the magnetic moment orientation, the dynamic magnetization, frequency-dependent susceptibility, and relaxation times of the particle's magnetic moments are determined. It is shown that the system's magnetic response is formed under the influence of competing interactions, such as dipole-dipole, field-dipole, and dipole-easy-axis interactions. The contribution of each interaction to the magnetic nanoparticle's dynamic response is analyzed. The obtained results provide a theoretical basis for predicting the properties of soft, magnetically sensitive composites, which are increasingly used in high-tech industrial and biomedical technologies.

DOI: [10.1103/PhysRevE.107.024601](https://doi.org/10.1103/PhysRevE.107.024601)

I. INTRODUCTION

Ensembles of immobilized magnetic nanoparticles (MNPs) are the basis for the modeling of the behavior of soft magnetically sensitive materials consisting of magnetic nanoparticles embedded in a soft polymer matrix. The rapid development of the experimental synthesis of magnetically sensitive composites over the past decade [1–8] is associated with the perspective of their application in many high-tech industrial and biomedical technologies [9–14]. This is because polymer materials possess a unique combination of extensive physical properties, the considerable response of magnetic fillers to a magnetic field, and the ability to control the electrical, magnetic, and other characteristics of these materials with an external field. The spatial arrangement of the magnetic filler particles and their orientation texturing created during the synthesis of the sample mainly determine the composite's behavior and the features of its reaction to a magnetic field [15–21].

Most of the known theoretical and numerical results for the dynamic magnetic response of immobilized MNPs to an ac magnetic field concern noninteracting samples. For example, in [5,22–26] the dynamic magnetic properties and characteristic relaxation times of systems of noninteracting immobilized MNPs with aligned easy axes were studied when the ac magnetic field was directed parallel or perpendicular to the easy axes. The effect of interparticle interactions on the dynamic susceptibility of immobilized MNPs with aligned easy axes was studied in [27,28], with the ac field

and the easy axes oriented parallel to each other. In the same system, heat generation under the influence of a magnetic field was studied in [29,30], while the influence of an ac magnetic field's amplitude on the dynamic susceptibility and characteristic relaxation times of particle magnetic moments was considered in [28,31].

This work is devoted to the theoretical study of the dynamic magnetic response of a system of immobilized interacting MNPs with the anisotropic orientation of the easy axes. We focus on a model in which magnetic nanoparticles are equally distributed and their easy axes are directed parallel to each other. A sketch of the system under consideration is shown in Fig. 1. Composites with the orientation texture described above can be obtained from the liquid dispersion of MNPs in a strong static magnetic field and followed by the polymerization or freezing of the carrier liquid [5,14,32]. After polymerization, the particles lose translational degrees of freedom and their reaction to magnetic fields occurs by Néel rotation, when the nanoparticle's magnetic moment deviates from the easy axis inside the particle's body. In this paper the features of the reaction of such samples to an ac magnetic field directed perpendicular to the easy axes are studied. The main focus is the analysis of the influence of interparticle dipole-dipole interactions and field amplitude on the magnetic properties and relaxation processes occurring in these systems.

II. MODEL AND THEORY

We consider an ensemble of identical spherical uniaxial MNPs uniformly distributed and immobilized in a matrix.

*Ekaterina.Elfimova@urfu.ru

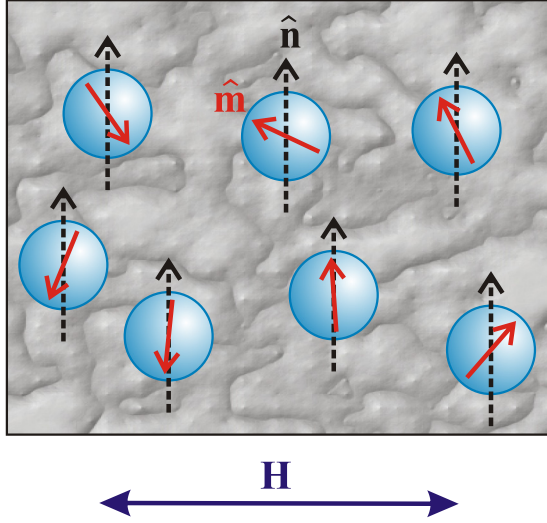


FIG. 1. Sketch of the sample considered here: a frozen configuration of magnetic nanoparticle positions and easy-axis orientations. The black dashed arrows show the easy-axis direction $\hat{\mathbf{n}}$, while the red solid arrows represent the magnetic moment orientation $\hat{\mathbf{m}}$; the ac magnetic field \mathbf{H} is directed perpendicular to the easy magnetization axes.

The translational and rotational degrees of freedom of the MPN bodies are turned off. The center position of each i th MNP is defined by its radius vector $\mathbf{r}_i = r_i(\sin \xi_i \cos \psi_i, \sin \xi_i \sin \psi_i, \cos \xi_i)$. Each MNP has a diameter d and the volume $v_m = \pi d^3/6$. The magnetic material of the MNPs is characterized by the bulk saturation magnetization M_s and the magnetic anisotropy constant K . So the MNP magnetic moment is $m = M_s v_m$. The MNP number concentration is ρ , while the volume fraction is $\varphi = \rho \pi d^3/6$. The direction of the particle's easy axis is defined by the unit vector $\hat{\mathbf{n}}$, and we consider the case when all particle easy axes are coaligned and parallel to the Oz axis; the vector $\hat{\mathbf{n}} = (0, 0, 1)$ is identical for all particles. The magnetic moment is able to rotate inside the MPN body through the Néel mechanism; the direction of the MNP magnetic moment $\mathbf{m}_i = m\hat{\mathbf{m}}_i = m(\sin \theta_i \cos \phi_i, \sin \theta_i \sin \phi_i, \cos \theta_i)$ differs from $\hat{\mathbf{n}}$. The laboratory coordinate system is presented in Fig. 2. Magnetic moment rotation is described the Néel energy U_N :

$$U_N(i) = -Kv_m(\hat{\mathbf{m}}_i \cdot \hat{\mathbf{n}})^2 = -Kv_m \cos^2 \theta_i. \quad (1)$$

We assume that the spherical particles are uniformly magnetized, so the magnetic interaction between them is described by the dipole-dipole potential without multipole corrections [33,34]

$$U_d(i, j) = -\frac{\mu_0 m^2}{4\pi r_{ij}^3} [3(\hat{\mathbf{m}}_i \cdot \hat{\mathbf{r}}_{ij})(\hat{\mathbf{m}}_j \cdot \hat{\mathbf{r}}_{ij}) - (\hat{\mathbf{m}}_i \cdot \hat{\mathbf{m}}_j)], \quad (2)$$

where μ_0 is the vacuum magnetic permeability, $\mathbf{r}_{ij} = \mathbf{r}_i - \mathbf{r}_j = r_{ij}\hat{\mathbf{r}}_{ij}$ is the center-center separation vector, and $r_{ij} = |\mathbf{r}_{ij}|$, $\hat{\mathbf{r}}_{ij}$ is the unit vector.

To avoid demagnetization corrections, we assume that the MNPs are contained in a long cylindrical tube oriented along the Oy axis and an ac magnetic field $\mathbf{H} = H \cos(\omega t)\hat{\mathbf{H}}$ is

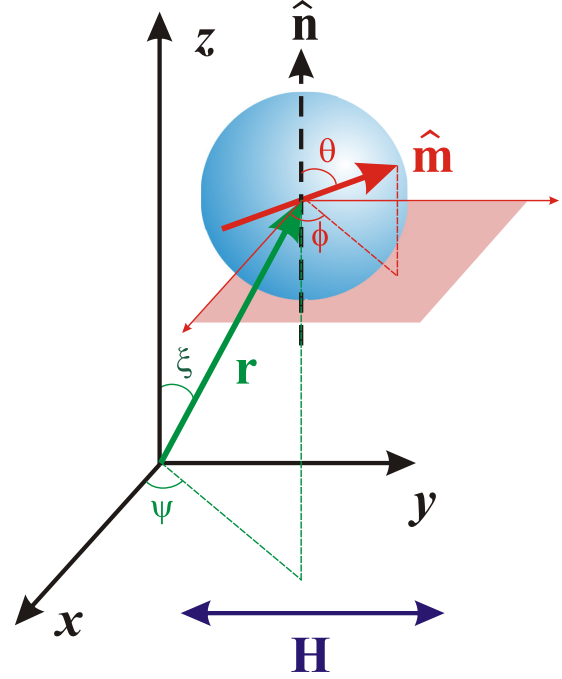


FIG. 2. Laboratory coordinate system. An immobilized particle's position is defined by radius vector $\mathbf{r} = r(\sin \xi \cos \psi, \sin \xi \sin \psi, \cos \xi)$. The particle's orientation is given by the magnetic easy-axis vector $\hat{\mathbf{n}} = (0, 0, 1)$ frozen in the particle's body. The particle magnetic moment's orientation is determined by the vector $\hat{\mathbf{m}} = (\sin \theta \cos \phi, \sin \theta \sin \phi, \cos \theta)$, which can differ from the easy-axis vector.

applied in the same direction, where H is the amplitude, $t = \bar{t}/2\tau_D$ is the time in units of the double effective relaxation time of the magnetic moment $2\tau_D$, $\omega = 2\tau_D\bar{\omega}$ is a reduced angular frequency of the field, and $\hat{\mathbf{H}} = (0, 1, 0)$. In this case, the internal macroscopic field inside the sample is equal to the external magnetic field \mathbf{H} . The interaction $U_m(i)$ between the magnetic moment of the i th MNP and the magnetic field can be written in a Zeeman form

$$U_H(i) = -\mu_0(\mathbf{m}_i \cdot \mathbf{H}) = -\mu_0 m H \cos(\omega t) \sin \theta_i \sin \phi_i. \quad (3)$$

The orientation of each magnetic moment is denoted by the probability distribution function $W = W(t, x, \phi)$, $x = \cos \theta_i$ which is the solution of the Fokker-Plank equation (FPE)

$$\frac{\partial W}{\partial t} = \frac{\partial}{\partial x} \left[(1-x^2) \left(\frac{\partial W}{\partial x} + W \frac{\partial U}{\partial x} \right) \right] + \frac{1}{1-x^2} \frac{\partial}{\partial \phi} \left(\frac{\partial W}{\partial \phi} + W \frac{\partial U}{\partial \phi} \right), \quad (4)$$

where U is the system's potential energy in units of the thermal energy $k_B T$. Here W satisfies the normalization condition

$$\int_0^{2\pi} \int_{-1}^1 W(t, x, \phi) dx d\phi = 1. \quad (5)$$

For an ideal case of noninteracting MNPs, the system's potential energy is

$$U = U_{id} = \frac{U_N(i) + U_H(i)}{k_B T}. \quad (6)$$

For interacting MNPs, we use the approximation suggested in [35], where dipole-dipole interactions are taken into account within the framework of first-order modified mean-field (MMF1) theory [36]:

$$U = U_{int} = \frac{1}{k_B T} [U_N(i) + U_H(i) + \rho \langle U_d(ij) W^{id}(j) \Theta(ij) \rangle_j]. \quad (7)$$

Here the Heaviside step function $\Theta(ij)$ describes the impenetrability of two MNPs, while $W^{id}(j)$ is the orientational probability for the magnetic moment of the particle j in an ideal (noninteracting) system. The angular brackets denote the integration over the positions of particle j and its magnetic moment orientations

$$\langle \dots \rangle_j = \int d\mathbf{r}_j d\hat{\mathbf{m}}_j, \quad \int d\hat{\mathbf{m}}_j = \frac{1}{4\pi} \int_{-1}^1 d \cos \theta_j \int_0^{2\pi} d\phi, \quad (8)$$

$$\int d\mathbf{r}_j = \lim_{R \rightarrow \infty} \int_0^{2\pi} d\psi_j \int_{-1}^1 d \cos \xi_j \int_0^{R/\sin \xi_j} r_j^2 dr_j. \quad (9)$$

It should be noted that MMF1 theory takes into account only coupled interparticle dipole-dipole correlations, so it has limitations when applied. Testing MMF1 theory through the results of a computer simulation has shown that it is valid for predicting the properties of MNPs with $\chi_L \lesssim 2$ [37].

Substituting the expressions (1)–(3) into (7) and performing integration through translational degrees of freedom of the j th particle (9), the potential energy of the system takes the form

$$U = U_{int} = - \left(\sigma \cos^2 \theta_i + \alpha \cos(\omega t) \sin \theta_i \sin \phi_i + \frac{\chi_L}{2} \int W^{id}(2) [3m_{1z} m_{2z} - (\hat{\mathbf{m}}_1 \cdot \hat{\mathbf{m}}_2)] d\hat{\mathbf{m}}_2 \right), \quad (10)$$

where $\alpha = \mu_0 m H / k_B T$ is a Langevin parameter characterizing the dipole-field interactions, $\sigma = K v_m / k_B T$ is the magnetocrystalline anisotropy parameter, and $\chi_L = 8\phi\lambda$ is

the Langevin susceptibility, which is a complex characteristic of the sample density φ and the intensity of interparticle dipole-dipole interactions $\lambda = \mu_0 m^2 / 4\pi d^3 k_B T$; m_{iz} is the z component of the vector $\hat{\mathbf{m}}_i$. The dynamic magnetization $M(t)$ and susceptibility $\chi(\omega)$ are determined in the standard way:

$$M(t) = \rho m \int d\hat{\mathbf{m}}_i (\hat{\mathbf{m}}_i \cdot \hat{\mathbf{H}}) W = \frac{\rho m}{4\pi} \int_0^{2\pi} \int_0^\pi W \sin^2 \theta \sin \phi d\theta d\phi, \quad (11)$$

$$\text{Re}(\chi) = \frac{\omega}{\pi H} \int_0^{2\pi/\omega} M(t) \cos(\omega t) dt,$$

$$\text{Im}(\chi) = \frac{\omega}{\pi H} \int_0^{2\pi/\omega} M(t) \sin(\omega t) dt. \quad (12)$$

III. NUMERICAL MODELING

A. Numerical solution of the Fokker-Plank equation

To solve the FPE (4) we use the finite-difference scheme proposed in [38]. This method's advantage is numerical stability, even when convection terms containing the system's energy predominate in the FPE. The scheme's unconditional stability and the criteria of the convergence of the numerical approximation to the solution were proved in [38]. This numerical algorithm has already been successfully applied to solve the FPE for interacting moving single-domain magnetic particles [39] and immobilized MNPs whose easy axes are aligned parallel to an ac magnetic field [28]. This algorithm's features and basic elements when an ac magnetic field is directed perpendicular to the easy axes are outlined here.

A three-dimensional space (t, x, ϕ) was split into a uniform grid $\{(t_k, x_i, \phi_j) \mid t_k = t_{k-1} + h_t, x_i = x_{i-1} + h_x, \phi_j = \phi_{j-1} + h_\phi, t_0 = 0, x_0 = -1 + h_x/2, \phi_0 = h_\phi/2\}$, with a finite number of nodes. Here h_t , h_x , and h_ϕ determine grid cell size in the t , x , and ϕ directions. Indices k , i , and j vary from 0 to their final values $N_t = T_f/h_t$, $N_x = 2/h_x - 1$, and $N_\phi = 2\pi/h_\phi - 1$, correspondingly, where T_f is the final moment of time in the calculation. Using the notation $W_{i,j}^k = W(t_k, x_i, \phi_j)$, the FPE (4) can be represented in discrete form as a convection-diffusion equation

$$\frac{\exp(-\delta h_t) W_{i,j}^k - W_{i,j}^{k-1}}{h_t} + (C_2 + D + \delta) [\exp(-\delta h_t) W^k(x, \phi)] = 0, \quad k = 0, \dots, N_t, \quad i = 0, \dots, N_x, \quad j = 0, \dots, N_\phi. \quad (13)$$

Here D and C_2 are discrete operators for the diffusion and convection terms accordingly. For the operator D , the standard second-order central difference is used,

$$DW^k(x, \phi) = \frac{1}{h_x^2} \left[-f_1 \left(x_i + \frac{h_x}{2} \right) (W_{i+1,j}^k - W_{i,j}^k) + f_1 \left(x_i - \frac{h_x}{2} \right) (W_{i,j}^k - W_{i-1,j}^k) \right] + \frac{1}{h_\phi^2} \left[-f_2(x_i) (W_{i,j+1}^k - W_{i,j}^k) + f_2(x_i) (W_{i,j}^k - W_{i,j-1}^k) \right],$$

where $f_1(x) = 1 - x^2$ and $f_2(x) = 1/(1 - x^2)$. The operator C_2 is constructed to satisfy the stability criteria of the numerical solution and is defined as follows:

$$C_2 W^k(x, \phi) = \frac{1}{2h_x} [v_1(t^*, x_i + 0.5h_x, \phi_j)(W_{i+1,j}^k + W_{i,j}^k) - v_1(t^*, x_i - 0.5h_x, \phi_j)(W_{i,j}^k + W_{i-1,j}^k)] + \frac{1}{2h_\phi} [v_2(t^*, x_i, \phi_j + 0.5h_\phi)(W_{i,j}^k + W_{i,j+1}^k) - v_2(t^*, x_i, \phi_j - 0.5h_\phi)(W_{i,j}^k + W_{i,j-1}^k)],$$

$$t^* = \frac{t_{k+1} + t_k}{2}, \quad v_1(t, x, \phi) = \frac{\partial U(1)}{\partial x}, \quad v_2(t, x, \phi) = \frac{\partial U(1)}{\partial \phi}.$$

In Eq. (13), δ is a regularization parameter that is used to make the numerical scheme unconditionally stable; it is equal to $\delta = 0.5 \max |(v_1)'_x + (v_2)'_\phi|$.

Using the classical difference scheme of alternating directions (the Peaceman-Rachford scheme), Eq. (13) is reduced to a system of discrete equations

$$\frac{u^{k+1/2} - u^k}{0.5h_t} + \Lambda_1 u^{k+1/2} + \Lambda_2 u^k = 0, \quad \frac{u^{k+1} - u^{k+1/2}}{0.5h_t} + \Lambda_1 u^{k+1/2} + \Lambda_2 u^{k+1} = 0, \tag{14}$$

where $u^k = e^{\delta h_t} W^k$, Λ_1 is the difference operator in variable x , and Λ_2 is the difference operator in variable ϕ . At every $t = t_k$ each equation of the system (14) is a linear algebraic system solved by the tridiagonal matrix algorithm. To satisfy the condition (5), normalization is performed

$$W_{i,j}^{k,\text{norm}} = \frac{W_{i,j}^k}{h_x h_\phi \sum_{i=0}^{N_x} \sum_{j=0}^{N_\phi} W_{i,j}^k}.$$

Therefore,

$$h_x h_\phi \sum_{i=0}^{N_x} \sum_{j=0}^{N_\phi} W_{i,j}^{k,\text{norm}} = 1.$$

This equation is condition (5) in a discrete form, determined by the rectangle method. Magnetization M is calculated by integrating with the trapezoidal rule expression

$$M(t_k) = \frac{\rho m}{4\pi} \int_0^{2\pi} \int_{-1}^1 W^{\text{norm}}(t_k, x, \phi) x dx d\phi, \quad x \in \{x_i\}, \quad \phi \in \{\phi_j\}. \tag{15}$$

The real $\text{Re}(\chi)$ and imaginary $\text{Im}(\chi)$ parts of the susceptibility can be found by the numerical integration of (12) over $\{t_k\}$.

B. Testing numerical results

To test the algorithm the FPE was first solved numerically for a number of special cases where there are known analytical approximations of the dynamic susceptibility.

(i) A theory of the dynamic magnetic response of an ensemble of immobilized MNPs to an ac magnetic field with a low amplitude was developed in [40]. This theory is based on the FPB equation for the case when the easy axes are aligned in one direction and the ac field is oriented at a given angle to the easy axes. Following [40], the susceptibility of the noninteracting χ_\perp^{id} and the interacting χ_\perp MNPs in the ac field directed perpendicular to the easy axes can be written as

$$\chi_\perp^{id} = B_1^{id} \chi_L, \quad \chi_\perp = \chi_L B_1^{id} \left(1 + \frac{\chi_L B_1^{id}}{3} \right), \tag{16}$$

where B_1^{id} is found from the solution to the set of equations

$$\left[2\tau_D i\omega + n(n+1) - 2\sigma \frac{n^2 + n - 3}{(2n-1)(2n+3)} \right] B_n^{id} - 2\sigma \frac{(n-2)(n-1)(n+1)}{(2n-3)(2n-1)} B_{n-2}^{id} + 2\sigma \frac{n(n+2)(n+3)}{(2n+3)(2n+5)} B_{n+2}^{id} = \frac{2(2n+1)(n-1)!}{(n+1)!} \left(\int_{-1}^1 e^{\sigma x^2} dx \right)^{-1} \int_{-1}^1 e^{\sigma x^2} \sqrt{1-x^2} (1+\sigma x^2) P_n^1(x) dx. \tag{17}$$

Here $P_n^1(x)$ is the first associated Legendre polynomial. Explicit expressions for B_1^{id} can be determined by truncating $n = l$ at some arbitrary order setting $B_{n>l}^{id} = 0$ and solving the set of l algebraic equations. It is worth noting

that the formulas (16) and (17) are valid only for low-field amplitudes.

(ii) In the case $\sigma = 0$, the results of the numerical solution of the FPE can be compared with a theory

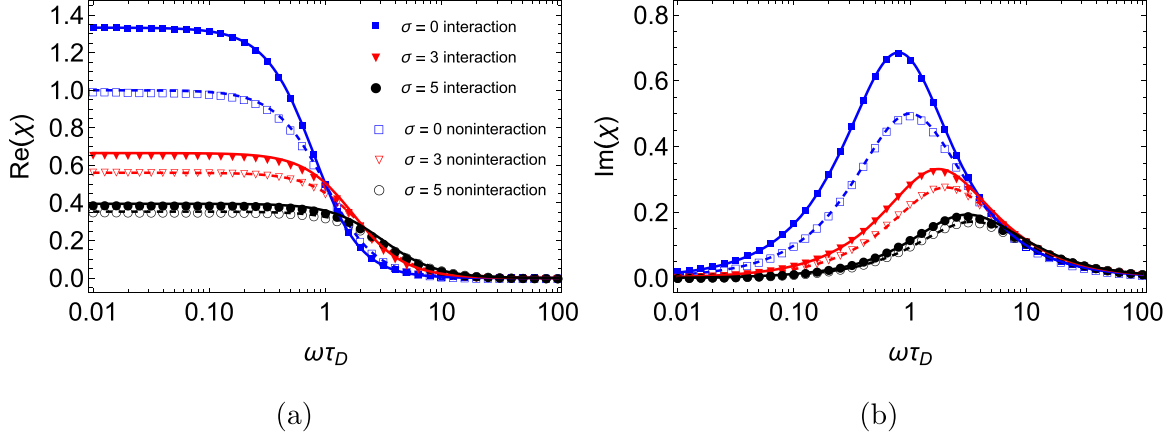


FIG. 3. Real and imaginary parts of the susceptibility for noninteracting (dashed lines and open symbols) and interacting (solid lines and closed symbols) immobilized MNPs with $\chi_L = 1$ at $\alpha = 0.01$. Lines correspond to analytical expressions (16) and (17) from [40] obtained for low-field amplitudes. The symbols are from numerical solution of the FPE. The anisotropy constants are $\sigma = 0$ (blue squares), $\sigma = 3$ (red triangles), and $\sigma = 5$ (black circles).

developed for a system of moving particles. At $\sigma = 0$, the magnetic moment rotates easily inside the particle's body, which corresponds to the rotation of the particle itself. The arrangement of particles in systems of moving and immobilized MNPs is indistinguishable from the theoretical point of view, since it is random and uniform. In Ref. [41], based on rigorous statistical and mechanical principles, it was shown that the expression for the static magnetization of immobilized MNPs at $\sigma \rightarrow 0$ is the same as the magnetization of a ferrofluid. In addition, Ref. [41] derived analytical formulas of static magnetization and susceptibility for ensembles of immobilized magnetic particles with the easy axes distributed according to particular textures; these are aligned parallel or perpendicular to an external magnetic field or randomly distributed. In this section a comparison of numerical results for a system with $\sigma = 0$ is carried out with two theories. The first theory [42] is valid for a system of noninteracting moving MNPs in an ac magnetic field with an arbitrary amplitude:

$$\begin{aligned} \text{Re}(\chi) &= \frac{\chi(0)}{1 + (\omega\tau_e)^2}, \quad (18) \\ \text{Im}(\chi) &= \frac{\chi(0)\omega\tau_e}{1 + (\omega\tau_e)^2} \left(1 + \frac{0.024\alpha^2}{1 + 0.18\alpha + 0.033\alpha^2} \right), \\ \tau_e &= \frac{\tau_D}{\sqrt{1 + 0.07\alpha^2}}, \\ \frac{\chi(0)}{\chi_L} &= 1 - \frac{0.0636\alpha^2}{1 + 0.18\alpha + 0.0659\alpha^2}. \quad (19) \end{aligned}$$

The second theory [39] was developed for interacting, moving MNPs in an ac field with an arbitrary amplitude:

$$\begin{aligned} \text{Re}(\chi) &= \frac{\chi^*(0)}{1 + (\omega\tau_e^*)^2}, \quad (20) \\ \text{Im}(\chi) &= \frac{\chi^*(0)\omega\tau_e^*}{1 + (\omega\tau_e^*)^2} \left(1 + \frac{0.027\alpha^2}{1 + 0.102\alpha + 0.047\alpha^2} \right), \quad (21) \end{aligned}$$

$$\begin{aligned} \chi^*(0) &= \chi_L \left(1 + \frac{\chi_L}{3} \right) \left(1 - \frac{0.101\alpha^2}{1 + 0.276\alpha + 0.104\alpha^2} \right), \\ \frac{1}{\tau_e^*} &= \frac{1}{\tau_D} \sqrt{\left(1 - \frac{\chi_L}{3} \right)^2 + 0.076\alpha^2}. \end{aligned}$$

A comparison of the numerical results of the FPE solution with theories (16)–(21) is presented in Figs. 3 and 4. The theoretical results are indicated by lines, while the numerical data are shown by symbols. To numerically calculate the dynamic susceptibility of noninteracting MNPs we use the single-particle potential (6). To calculate the magnetic response of interacting MNPs, the potential energy (10), which takes into account dipole-dipole interactions, was substituted into the FPE. The numerical calculation was carried out on a grid of size $h_t = 0.001$ and $h_x = h_\phi = 0.01$. To test the numerical algorithm on theories (16) and (17), the amplitude of the ac field was equal to $\alpha = 0.01$ in the numerical calculations (Fig. 3). When comparing the numerical results with theories (18)–(21), the magnetic anisotropy constant σ was equal to zero (Fig. 4). There is good agreement between the numerical and analytical results for both noninteracting and interacting MNPs. It should also be noted that an increase in the magnetic anisotropy constant σ leads to a significant decrease in the system's magnetic response in the frequency range $\omega\tau_D \lesssim 2$ (Fig. 3). An increase in field amplitude leads to a decrease in the dynamic susceptibility for any frequency of the ac field (Fig. 4). Dipole-dipole interactions lead to an increase in the magnetic response of MNPs. These trends will be discussed in the next section in detail.

IV. RESULTS AND DISCUSSION

A. Role of interparticle interactions

Figure 5 shows the frequency dependence of the real and imaginary parts of the dynamic susceptibility for noninteracting (dashed lines) and interacting (solid lines) MNPs with a

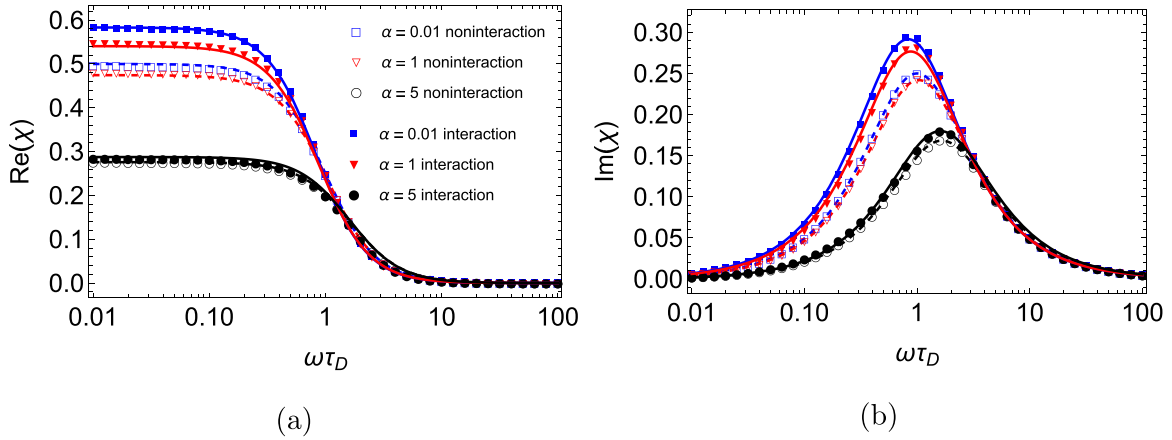


FIG. 4. Numerical results of the real and imaginary parts of the susceptibility for noninteracting (open symbols) and interacting (closed symbols) immobilized MNPs with $\chi_L = 0.5$ and $\sigma = 0$. The numerical data are compared with the theory developed for mobile MNPs: Dashed lines correspond to the analytical expressions (18) and (19) from [42] obtained for noninteracting MNPs; solid lines show the theory for interacting MNPs (20) and (21) from [39]. The Langevin parameters are $\alpha = 0.01$ (blue), $\alpha = 1$ (red), and $\alpha = 5$ (black).

Langevin susceptibility $\chi_L = 0.1, 1$, and 1.5 at $\alpha = 1$ and $\sigma = 1$. Interparticle interactions increase the magnetic response of immobilized MNPs, and at greater χ_L the contribution of dipole-dipole interactions to the dynamic susceptibility are more pronounced. This behavior is due to the fact that dipole-dipole interactions contribute to the formation of the head-to-tail correlated magnetic moment structures oriented along the field direction, which leads to an increase in the system's susceptibility. Correlated magnetic moments react more slowly to the ac magnetic field, which is indicated by the left shift of the maximum of the imaginary part of the susceptibility of interacting MNPs with an increase in χ_L .

Figure 6 shows the contour plots of the ratio of the susceptibility χ of interacting MNPs to the susceptibility χ_{id} of MNPs without interactions depending on field amplitude α and the magnetic anisotropy constant σ in the ac field's low-frequency region of $\omega \rightarrow 0$. The figures show the effect of interparticle dipole-dipole interactions on the static susceptibility of immobilized MNPs. Blue corresponds to the value $\chi/\chi_{id} \approx 1$. In these regions, interparticle dipole-dipole interactions do not contribute to susceptibility; its value is determined mainly by dipole-field and dipole-easy-axis interactions. It can be

seen that for a system with weak interparticle interactions ($\chi_L = 0.5$) the region in which $\chi/\chi_{id} > 1$ is limited by lower values of α and σ in comparison with a system with stronger interparticle interactions ($\chi_L = 1.5$). In all cases, interparticle dipole-dipole interactions make the greatest contribution to the susceptibility of immobilized MNPs at low values of field amplitude α and the magnetic anisotropy constant σ .

Figure 7 shows the inverse value of the maximum position of the imaginary part of susceptibility $1/\omega_{\max}\tau_D$ depending on the field amplitude α and the magnetic anisotropy constant σ at $\chi_L = 1.5$. The value $1/\omega_{\max}\tau_D$ determines the ratio of the effective relaxation time τ_{relax} of the magnetic moment of interacting immobilized MNPs to the characteristic time τ_D . Note that τ_D describes relaxation processes associated with the thermal fluctuations of the magnetic moment that occur inside a single MNP when $\sigma \ll 1$. This time is determined by the formula [43,44] $\tau_D = \sigma\tau_0$, where $\tau_0 = m/2a\gamma Kv_m$ is the precession damping time, a the spin-lattice relaxation parameter, and γ the gyromagnetic ratio. An increase in σ and α accelerates relaxation processes in a system of immobilized MNPs, while interparticle dipole-dipole interaction slows them down. At certain values of parameters α and σ ,

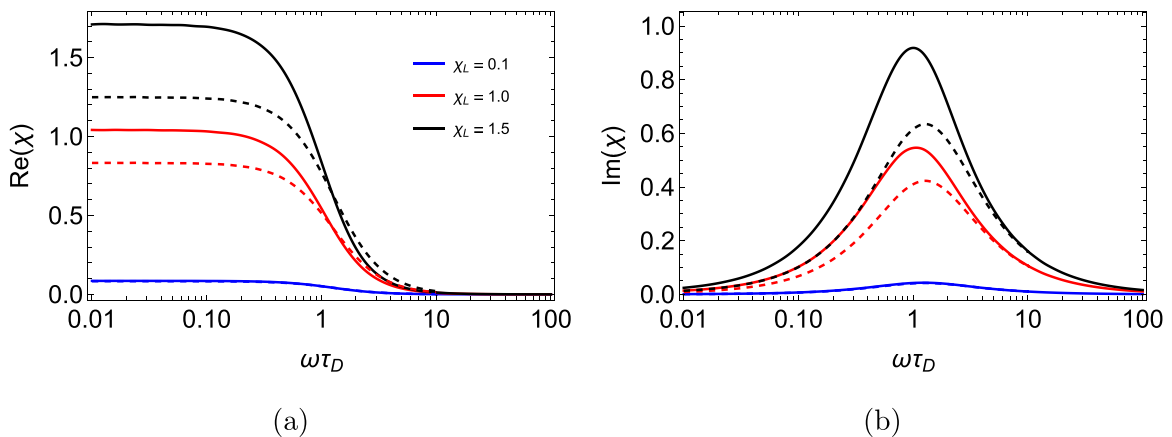


FIG. 5. Real and imaginary parts of the susceptibility for noninteracting (dashed lines) and interacting (solid lines) particles at $\alpha = 1$, $\sigma = 1$, and different values of the Langevin susceptibility $\chi_L = 0.1, 1$, and 1.5 .

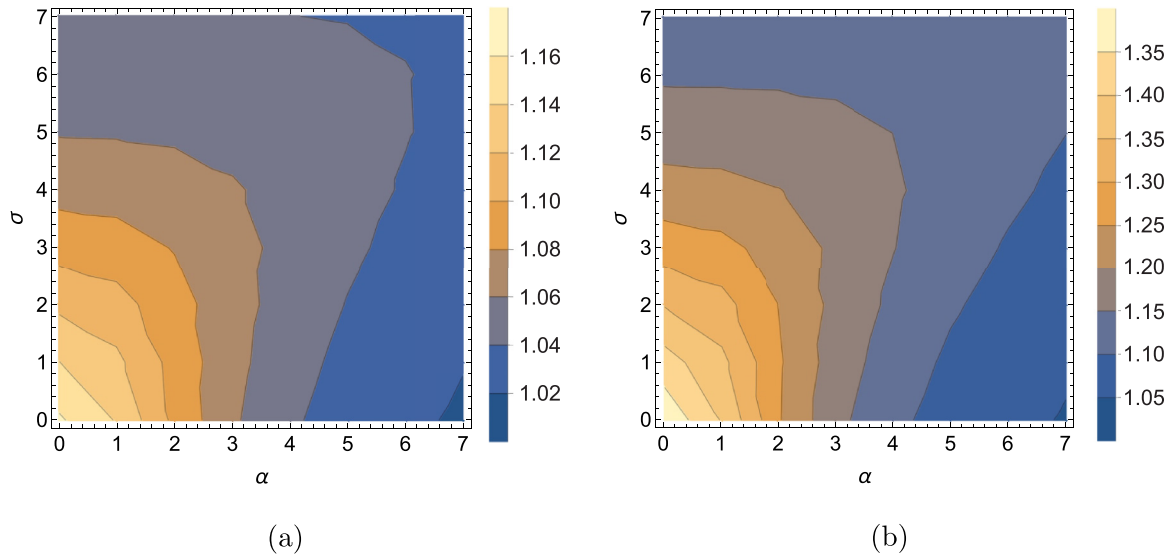


FIG. 6. Contour plots of the ratio $\chi(\omega \rightarrow 0)/\chi_{id}(\omega \rightarrow 0)$ depending on field amplitude α and magnetic anisotropy constant σ at (a) $\chi_L = 0.5$ and (b) $\chi_L = 1.5$.

these effects compensate for each other; as a result, the value of τ_{relax}/τ_D becomes equal to 1.

The effect of interparticle interactions on the effective relaxation time of the magnetic moment for immobilized MNPs is shown in Fig. 8. The ratio of the magnetic moment relaxation time τ_{relax} of interacting MNPs to the relaxation time τ_{relax}^{id} of noninteracting MNPs τ_{relax}^{id} is presented depending on σ for three different values $\chi_L = 0.5, 1.0,$ and 1.5 at $\alpha = 1$. The values of τ_{relax} and τ_{relax}^{id} were calculated from the position of the maximum of the imaginary part of the dynamic susceptibility. It can be seen that interparticle interactions slow down relaxation processes, however, with an increase in σ the ratio $\tau_{relax}/\tau_{relax}^{id} \rightarrow 1$. This indicates a decrease of the influence of dipole-dipole interactions on the relaxation times of the magnetic moment and domination of the dipole-field and the dipole-easy-axis interactions.

The dynamic hysteresis loops for the system with $\chi_L = 1.5$ and $\sigma = 1$ at $\omega\tau_D = 0.1, 1,$ and 10 are shown in Fig. 9. The solid lines correspond to interacting MNPs, while dotted line shows the system without interactions. At the frequency $\omega\tau_D = 0.1$, the magnetic moment relaxation time is comparable to the field rate, so the magnetic moments have time to react to the field. This is indicated by the following factors. At $H^* = 1$, magnetization reaches its maximum value; the hysteresis loop is quite narrow. At $H^* = 0$ the magnetization value is close to zero. Dipole-dipole interactions have a significant effect on the system’s magnetization in the region of low-field frequencies. It can be seen that the slope of the hysteresis loop for interacting MNPs differs from that for noninteracting MNPs. With an increase in the frequency of the field $\omega\tau_D = 1$, there is an expansion of the hysteresis loop and a shift in the maximum value of magnetization to the region $H^* < 1$, which indicates a delay in the reaction of magnetic moments to the magnetic field rate. At $\omega\tau_D = 1$ the effect of dipole-dipole interactions on the system’s magnetization is still quite clearly expressed. In the high-frequency field

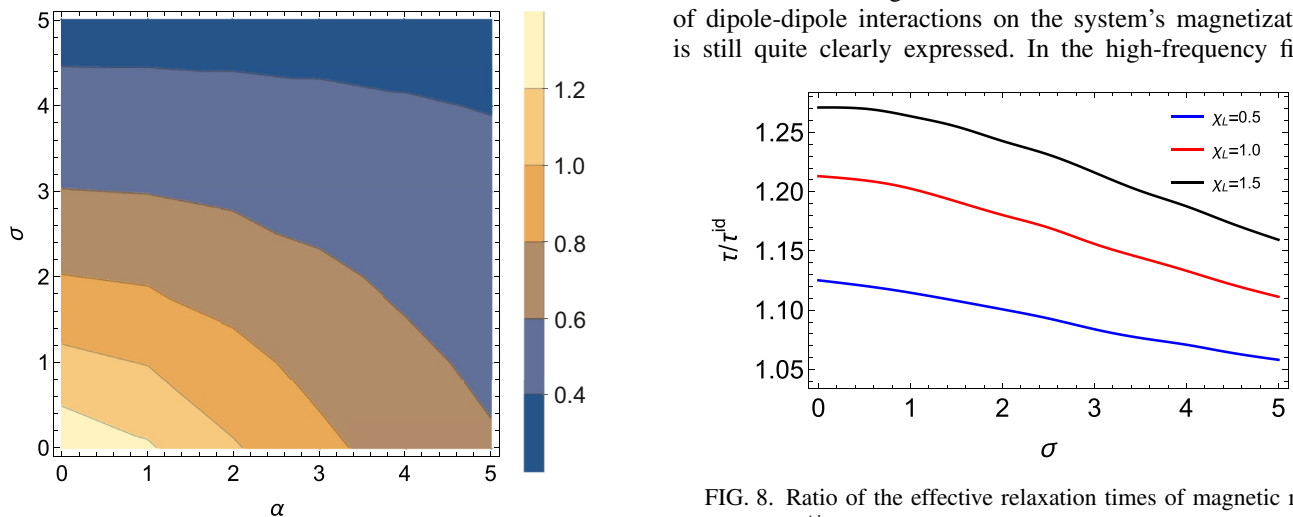


FIG. 7. Contour plots $1/\omega_{max} \tau_D = \tau_{relax} \tau_D$ depending on field amplitude α and magnetic anisotropy constant σ for immobilized interacting MNPs at $\chi_L = 1.5$.

FIG. 8. Ratio of the effective relaxation times of magnetic moments $\tau_{relax}/\tau_{relax}^{id}$ depending on σ for immobilized MNPs in an ac magnetic field with amplitude $\alpha = 1$. The blue line corresponds to a system with a Langevin susceptibility $\chi_L = 0.5$, the red line to $\chi_L = 1.0$, and the black line to $\chi_L = 1.5$.

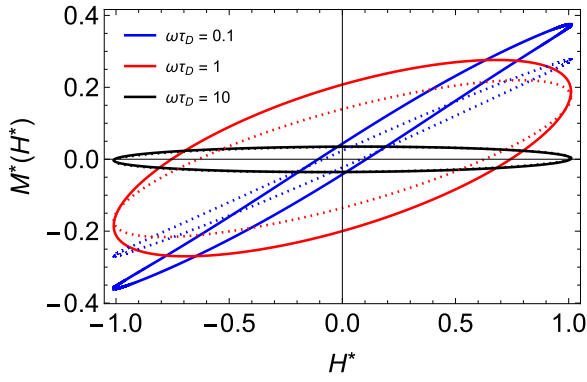


FIG. 9. Dynamic hysteresis loop $M^*(H^*) = M(H^*)/\rho m$, where $H^* = \alpha \cos \omega t$ for noninteracting MNPs (dotted line) and interacting MNPs (solid line) with $\chi_L = 1.5$, $\sigma = 1$, and $\alpha = 1$ at $\omega\tau_D = 0.1, 1$, and 10.

$\omega\tau_D = 10$ the hysteresis loop is located horizontally; at the maximum field $H^* = 1$ the magnetization is $M^* = 0$. The effect of dipole-dipole interactions on the system’s magnetization is absent. This indicates a strong delay in the magnetic moments behind the field rate.

B. Field amplitude effects

Figure 10 shows the effect of the amplitude of the ac magnetic field on the dynamic susceptibility of immobilized

interacting MNPs with $\chi_L = 1$ at different values of $\sigma = 1$ and 5. An increase in α leads to the system’s magnetization; therefore, its susceptibility to the ac field decreases. The value of σ determines the magnitude of the potential barrier that the magnetic moment must overcome to deviate from the easy axis. Therefore, the growth of σ prevents the reaction of the magnetic moment to the external field and the orientation of the magnetic moments along the field. This means that an increase in σ leads to a decrease in system susceptibility. This behavior is fundamentally different from the susceptibility of interacting immobilized MNPs, whose easy axes are aligned along the ac magnetic field [28]. In [28] it was shown that an increase in σ leads to an increase in the susceptibility of MNPs, since at high values of σ the magnetic moments cannot deviate from the easy axis and are aligned along the field. Figure 10 shows that at $\sigma = 5$ the susceptibility changes insignificantly with an increase in the field amplitude from $\alpha = 0.1$ to 5, which indicates the dominance of dipole–easy-axis interaction over dipole–field interaction.

Figure 11 shows the dynamic hysteresis loops characterizing the magnetization of the MNPs with $\chi_L = 1$ and $\sigma = 1$ in the ac field with an amplitude of $\alpha = 1, 2$, and 5 at different frequencies of the alternating field $\omega\tau_D = 0.1$ [Fig. 11(a)] and $\omega\tau_D = 1$ [Fig. 11(b)]. When $\omega\tau_D = 0.1$ and $\alpha = 5$, the output of the hysteresis loop to saturation is observed. This is due to the combination of two effects: A high-field amplitude supports the system’s magnetization, while a low-field frequency

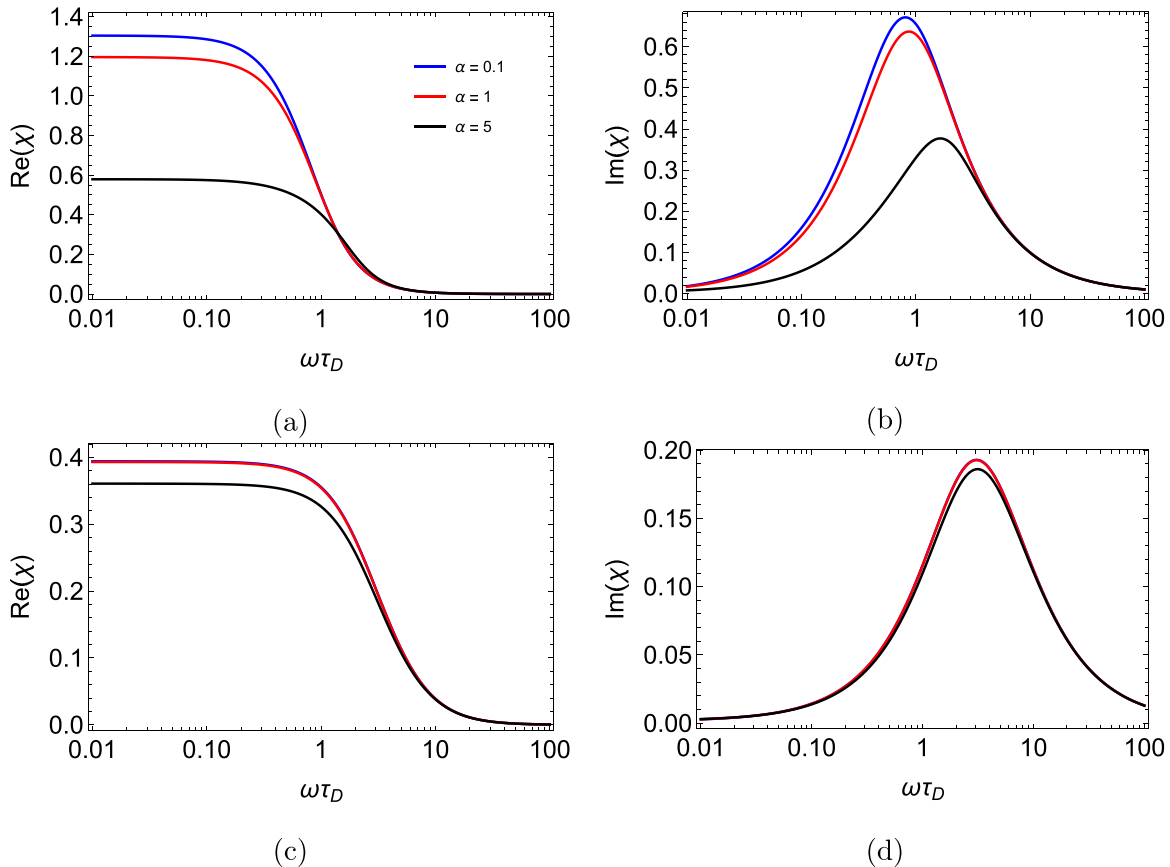


FIG. 10. Real and imaginary parts of the susceptibility with $\chi_L = 1$ at field amplitude $\alpha = 0.1, 1$, and 5 with (a) and (b) $\sigma = 1$ and (c) and (d) $\sigma = 5$.

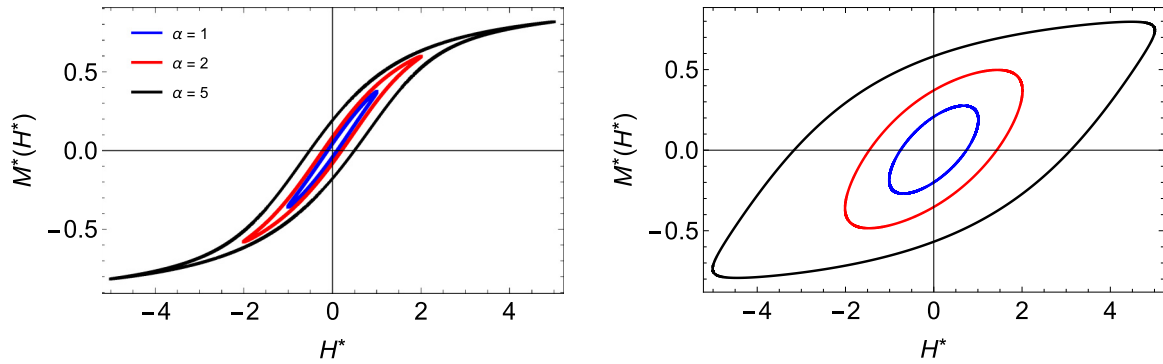


FIG. 11. Dynamic hysteresis loops for the immobilized interacting MNPs with $\chi_L = 1$ and $\sigma = 1$ in an ac magnetic field with frequency (a) $\omega\tau_D = 0.1$ and (b) $\omega\tau_D = 1$. Blue corresponds to the amplitude of the field $\alpha = 1$, red to $\alpha = 2$, and black to $\alpha = 5$.

allows magnetic moments to have time to respond to changes in the field. In general, an increase in field amplitude leads to an increase in the system's magnetization and the expansion of the hysteresis loop.

Figure 12 shows the dependence of the ratio of relaxation times $\tau_{\text{relax}}/\tau_D$ on ac field amplitude. The value of relaxation times was determined by the position of the maximum of the imaginary part of the dynamic susceptibility. An increase in field amplitude as well as an increase in the value of σ leads to a decrease in the ratio of $\tau_{\text{relax}}/\tau_D$; moreover, for some values of α and σ , this ratio becomes equal to one, that is, $\tau_{\text{relax}} = \tau_D$. The difference between τ_{relax} and τ_D is caused by the presence of competing interactions in the system, such as interparticle dipole-dipole interactions, which leads to an increase in τ_{relax} and the field-dipole and dipole-easy-axis interactions that contribute to a decrease in τ_{relax} . In some parameters, one type of interaction becomes dominant and completely determines the system's behavior.

V. CONCLUSION

This work investigated the properties of an ensemble of immobilized interacting MNPs with aligned easy axes. This system's magnetic response to an ac magnetic field directed perpendicular to the easy axes was studied. The reaction of MNPs to the field occurred via the Néel mechanism. Based on

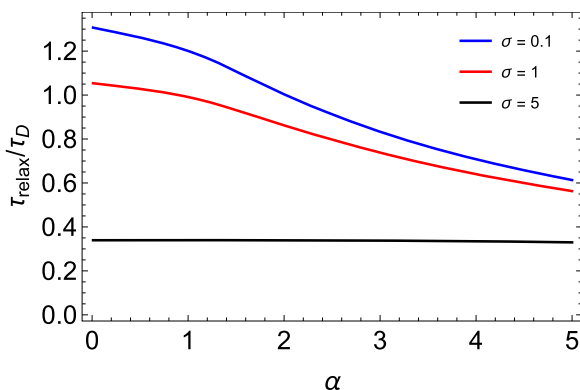


FIG. 12. Ratio $\tau_{\text{relax}}/\tau_D$ for immobilized interacting MNPs with $\chi_L = 1$ as a function of field amplitude α at $\sigma = 0.1, 1$, and 5 .

a numerical solution of the FPE for the probability density of the magnetic moment orientation, the dynamic magnetization, frequency-dependent susceptibility, and relaxation times of the magnetic moments of the particles were determined. Interparticle dipole-dipole interactions were taken into account in the FPE within the framework of first-order modified mean-field theory; therefore, the results are valid for moderately concentrated systems with $\chi_L \leq 1.5$.

The contributions of dipole-dipole, dipole-field, and dipole-easy-axis interactions to the dynamic magnetic properties of the considered system were analyzed. It was shown that an increase in field amplitude and particle magnetic anisotropy leads to a decrease in the dynamic susceptibility of MNPs, while dipole-dipole interactions increase the magnetic response of MNPs. Thus, the dynamic behavior of the MNP ensemble was determined by competing interactions. The numerical results made it possible to predict the dynamic properties for various combinations of parameters χ_L , σ , α , and ω , and there were no restrictions on the values of σ , α , and ω . It was shown that at high values of α and σ dipole-dipole interactions cease to affect the system's magnetic response. For example, for an ensemble of MNPs with $\chi_L = 0.5$, this region corresponds to $\alpha > 4$ and $\sigma > 7$ for any ac field frequency. In some parameters, one type of interaction becomes dominant and completely determines the system's behavior. For instance, for MNPs with $\chi_L = 1$ and $\sigma = 5$, an increase in field amplitude in the region of $0 < \alpha < 5$ does not lead to changes in the characteristic times of the relaxation processes occurring in the system.

The theory proposed in the article allows us to calculate numerically the values of dynamic magnetization and susceptibility and to determine the relaxation times for the given orientation geometry of the sample, taking into account competing interactions. This provides a basis for predicting the dynamic properties of soft magnetically sensitive materials with a specific internal orientation structure.

ACKNOWLEDGMENTS

The authors gratefully acknowledge research funding from the Ministry of Science and Higher Education of the Russian Federation (Ural Mathematical Center Project No. 075-02-2022-877).

- [1] S. Wu, W. Hu, Q. Ze, M. Sitti, and R. Zhao, Multifunctional magnetic soft composites: A review, *Multifunct. Mater.* **3**, 042003 (2020).
- [2] U., J. Sutrisno, A. Purwanto, and S. Mazlan, Recent progress on magnetorheological solids: Materials, fabrication, testing, and applications, *Adv. Eng. Mater.* **17**, 563 (2015).
- [3] R. I. Baron, G. Biliuta, V. Socoliuc, and S. Coseri, Affordable magnetic hydrogels prepared from biocompatible and biodegradable sources, *Polymers* **13**, 1693 (2021).
- [4] S. Shah, D. Reeves, R. Ferguson, J. Weaver, and K. Krishnan, Mixed Brownian alignment and Néel rotations in superparamagnetic iron oxide nanoparticle suspensions driven by an ac field, *Phys. Rev. B* **92**, 094438 (2015).
- [5] T. Yoshida, Y. Matsugi, N. Tsujimura, T. Sasayama, K. Enpuku, T. Viereck, M. Schilling, and F. Ludwig, Effect of alignment of easy axes on dynamic magnetization of immobilized magnetic nanoparticles, *J. Magn. Magn. Mater.* **427**, 162 (2017).
- [6] S. Ikhaddalene, F. Zibouche, A. Ponton, A. Irekti, and F. Carn, Synthesis and rheological properties of magnetic chitosan hydrogel, *Per. Polytech. Chem. Eng.* **65**, 378 (2021).
- [7] B. Elder, R. Neupane, E. Tokita, U. Ghosh, S. Hales, and Y. Kong, Nanomaterial patterning in 3D printing, *Adv. Mater.* **32**, 1907142 (2020).
- [8] V. Socoliuc, D. Peddis, V. Petrenko, M. Avdeev, D. Susan-Resiga, T. Szabó, R. Turcu, E. Tombácz, and L. Vékás, Magnetic nanoparticle systems for nanomedicine—A materials science perspective, *Magnetochemistry* **6**, 2 (2020).
- [9] Y. Zhou, X. Zhao, J. Xu, Y. Fang, G. Chen, Y. Song, S. Li, and J. Chen, Giant magnetoelastic effect in soft systems for bioelectronics, *Nat. Mater.* **20**, 1670 (2021).
- [10] H. Lu, M. Zhang, Y. Yang, Q. Huang, T. Fukuda, Z. Wang, and Y. Shen, A bioinspired multilegged soft millirobot that functions in both dry and wet conditions, *Nat. Commun.* **9**, 3944 (2018).
- [11] L. Makarova, T. Nadzharyan, Y. Alekhina, G. Stepanov, E. Kazimirova, N. Perov, and E. Kramarenko, Magnetoactive elastomer as an element of a magnetic retina fixator, *Smart Mater. Struct.* **26**, 095054 (2017).
- [12] T. Becker, V. Böhm, J. Chavez Vega, S. Odenbach, Y. Raikher, and K. Zimmermann, Magnetic-field-controlled mechanical behavior of magneto-sensitive elastomers in applications for actuator and sensor systems, *Arch. Appl. Mech.* **89**, 133 (2019).
- [13] L. Sanchez, V. Alvarez, and J. Gonzalez, in *Handbook of Composites from Renewable Materials*, edited by V. K. Thakur, M. K. Thakur, and M. R. Kessler (Wiley, New York, 2017), Vols. 1–8.
- [14] S. Abramchuk, E. Kramarenko, G. Stepanov, L. Nikitin, G. Filipcsei, A. Khokhlov, and M. Zrínyi, Novel highly elastic magnetic materials for dampers and seals: Part I. Preparation and characterization of the elastic materials, *Polym. Adv. Technol.* **18**, 883 (2007).
- [15] T. Yoshida, T. Sasayama, and K. Enpuku, (Invited) Biological applications of magnetic nanoparticles for magnetic immunoassay and magnetic particle imaging, *ECS Trans.* **75**, 39 (2016).
- [16] E. A. Elfimova, L. Y. Iskakova, A. Y. Solovyova, and A. Y. Zubarev, Theory of static magnetization of magnetopolymer composites: The second virial approximation, *Phys. Rev. E* **104**, 054616 (2021).
- [17] A. Solovyova, S. Sokolsky, E. Elfimova, and A. Ivanov, The thermodynamic properties of soft magnetic materials containing superparamagnetic nanoparticles frozen in the nodes of the regular cubic lattice, *J. Nanopart. Res.* **23**, 139 (2021).
- [18] V. Kolesnikova, L. Makarova, A. Omelyanchik, K. Sobolev, D. Isaev, I. Alekhina, A. Komlev, V. Rodionova, and N. Perov, Magnetoactive elastomers based on ferromagnetic and ferroelectric particles: A FORC approach, *J. Magn. Magn. Mater.* **558**, 169506 (2022).
- [19] A. Omelyanchik, V. Antipova, C. Gritsenko, V. Kolesnikova, D. Murzin, Y. Han, A. V. Turutin, I. V. Kubasov, A. M. Kislyuk, T. S. Ilina, D. A. Kiselev, M. I. Voronova, M. D. Malinkovich, Y. N. Parkhomenko, M. Silibin, E. N. Kozlova, D. Peddis, K. Levada, L. Makarova, A. Amirov *et al.*, Boosting magnetoelectric effect in polymer-based nanocomposites, *Nanomaterials* **11**, 1154 (2021).
- [20] V. Zverev, M. Gupalo, N. Mauser, S. Kantorovich, and E. Novak, The influence of an applied magnetic field on the clusters formed by Stockmayer supracolloidal magnetic polymers, *J. Magn. Magn. Mater.* **521**, 167445 (2021).
- [21] A. Zakinyan and Y. Dikansky, Effect of microdrops deformation on electrical and rheological properties of magnetic fluid emulsion, *J. Magn. Magn. Mater.* **431**, 103 (2017).
- [22] Y. L. Raikher and V. I. Stepanov, Nonlinear dynamic susceptibilities and field-induced birefringence in magnetic particle assemblies, *Adv. Chem. Phys.* **129**, 419 (2004).
- [23] R. J. Deissler, Y. Wu, and M. A. Martens, Dependence of Brownian and Néel relaxation times on magnetic field strength, *Med. Phys.* **41**, 012301 (2014).
- [24] W. T. Coffey, P. J. Cregg, D. S. Crothers, J. T. Waldron, and A. W. Wickstead, Simple approximate formulae for the magnetic relaxation time of single domain ferromagnetic particles with uniaxial anisotropy, *J. Magn. Magn. Mater.* **131**, L301 (1994).
- [25] A. Aharoni, Effect of a magnetic field on superparamagnetic relaxation time, *Phys. Rev.* **177**, 793 (1969).
- [26] W. T. Coffey, P. J. Cregg, and Y. P. Kalmykov, in *Advances in Chemical Physics*, edited by I. Prigogine and S. A. Rice (Wiley, New York, 1993), Vol. LXXXIII.
- [27] P.-M. Déjardin, Magnetic relaxation of a system of superparamagnetic particles weakly coupled by dipole-dipole interactions, *J. Appl. Phys.* **110**, 113921 (2011).
- [28] A. V. Ambarov, V. S. Zverev, and E. A. Elfimova, Numerical modeling of the magnetic response of interacting superparamagnetic particles to an ac field with arbitrary amplitude, *Model. Simul. Mater. Sci. Eng.* **28**, 085009 (2020).
- [29] A. Y. Zubarev, L. Y. Iskakova, and A. F. Abu-Bakr, Magnetic hyperthermia in solid magnetic colloids, *Physica A* **467**, 59 (2017).
- [30] A. Y. Zubarev, Magnetic hyperthermia in a system of ferromagnetic particles, frozen in a carrier medium: Effect of interparticle interactions, *Phys. Rev. E* **98**, 032610 (2018).
- [31] V. Zverev, A. Dobrosrodova, A. Kuznetsov, A. Ivanov, and E. Elfimova, Computer simulations of dynamic response of ferrofluids on an alternating magnetic field with high amplitude, *Mathematics* **9**, 2581 (2021).
- [32] P. Tancredi, P. C. Rivas-Rojas, O. Moscoso-Londono, D. Muraca, M. Knobel, and L. M. Socolovsky, Size and doping effects on the improvement of the low-temperature magnetic properties of magnetically aligned cobalt ferrite nanoparticles, *J. Alloys Compd.* **894**, 162432 (2022).

- [33] V. N. Bagaev, Y. A. Buevich, and V. V. Tetyukhin, Theory of magnetostatic interaction and structuring in dispersed systems, *Magneto hydrodynamics* **22**, 146 (1986).
- [34] B. F. Edwards, D. M. Riffe, J.-Y. Ji, and W. A. Booth, Interactions between uniformly magnetized spheres, *Am. J. Phys.* **85**, 130 (2017).
- [35] A. O. Ivanov, V. S. Zverev, and S. S. Kantorovich, Revealing the signature of dipolar interactions in dynamic spectra of polydisperse magnetic nanoparticles, *Soft Matter* **12**, 3507 (2016).
- [36] A. Pshenichnikov, V. Mekhonoshin, and A. Lebedev, Magneto-granulometric analysis of concentrated ferrocolloids, *J. Magn. Magn. Mater.* **161**, 94 (1996).
- [37] T. M. Batrudinov, Y. E. Nekhoroshkova, E. I. Paramonov, V. S. Zverev, E. A. Elfimova, A. O. Ivanov, and P. J. Camp, Dynamic magnetic response of a ferrofluid in a static uniform magnetic field, *Phys. Rev. E* **98**, 052602 (2018).
- [38] N. Afanas-eva, P. N. Vabishchevich, and M. V. Vasil-eva, Unconditionally stable schemes for convection-diffusion problems, *Russ. Math.* **57**, 1 (2013).
- [39] M. S. Rusanov, V. S. Zverev, and E. A. Elfimova, The dynamic magnetic susceptibility of a ferrofluid: The influence of inter-particle interactions and ac field amplitude, *Phys. Rev. E* **104**, 044604 (2021).
- [40] A. V. Ambarov, V. S. Zverev, and E. A. Elfimova, Dynamic response of interacting superparamagnetic particles with aligned easy magnetization axes, *J. Magn. Magn. Mater.* **497**, 166010 (2020).
- [41] E. A. Elfimova, A. O. Ivanov, and P. J. Camp, Static magnetization of immobilized, weakly interacting, superparamagnetic nanoparticles, *Nanoscale* **11**, 21834 (2019).
- [42] T. Yoshida and K. Enpuku, Simulation and quantitative clarification of ac susceptibility of magnetic fluid in nonlinear Brownian relaxation region, *Jpn. J. Appl. Phys.* **48**, 127002 (2009).
- [43] W. Brown, Thermal fluctuations of a single-domain particle, *Phys. Rev.* **130**, 1677 (1963).
- [44] Y. L. Raikher and V. I. Stepanov, Physical aspects of magnetic hyperthermia: Low-frequency ac field absorption in a magnetic colloid, *J. Magn. Magn. Mater.* **368**, 421 (2014).